A&A manuscript no.
(will be inserted by hand later)

Your thesaurus codes are:
03(11.13.2; 11.19.3; 13.09.1; 13.18.1)

ASTRONOMY
AND
ASTROPHYSICS
1.2.2008

arXiv:astro-ph/9605118v1 20 May 1996

The FIR/radio correlation in starburst galaxies – constraints on starburst models

U. Lisenfeld@*, H.J. Völk, C. Xu

Max-Planck-Institut für Kernphysik, Postfach 10 35 80, D-69029 Heidelberg, Germany

Received 30 January 1996/ Accepted 22 April 1996

Abstract. This paper presents an analysis of the correlation between the far-infrared (FIR) and the radio emission of starburst galaxies. Data for interacting galaxies, many of which are undergoing a starburst, and for normal galaxies have been analysed and compared in order to test for any influence of the star-formation activity on the ratio between the FIR and the radio emission at 2.4 GHz, $q_{2.4\mathrm{GHz}}$. No statistically significant indication for such an influence has been found: There is neither a significant difference between $q_{2.4\mathrm{GHz}}$ of the two samples nor a dependence of this ratio on the starburst strength. This observational fact is unexpected because of the different physical conditions and the short time-scale of the star-formation activity in a starburst. In order to interprete the observations the FIR and the radio emission during a starburst have been modeled. The following conclusions could be drawn from the observed constancy of $q_{2.4\mathrm{GHz}}$: A strong and fast ($\approx 10^7$ yr) increase of the magnetic field at the beginning of the starburst is required in order to maintain a constant $q_{2.4\mathrm{GHz}}$. Otherwise the strong Inverse Compton losses that are due to the intense radiation field in a starburst would lower the synchrotron emission drastically resulting in a value of $q_{2.4\mathrm{GHz}}$ significantly higher than the observed one. Furthermore, the time-scale of the variation of the star-formation rate has to be longer than some 10^7 yr. For lower values the different time-scales of the FIR and the radio emission produce large fluctuations of $q_{2.4\mathrm{GHz}}$.

Key words: Galaxies: starburst – galaxies: magnetic fields – infrared: galaxies – radio continuum: galaxies

1. Introduction

Starburst galaxies are found to follow the tight correlation between the far-infrared (FIR) and the radio emission (Wunderlich et al. 1987; van den Driel et al. 1991; Franceschini et al. 1988a; Condon et al. 1991). Here, the correlation is even more unexpected than in normal galaxies (see Lisenfeld et al. 1995 for a discussion of normal galaxies) because of the following reasons. In starburst galaxies the different time-scales involved in the production of the radio and the FIR emissions become important: Whereas the FIR emission and the thermal radio emission are instantaneously related to the stellar radiation, the synchrotron emission shows a time delay because it takes some 10^6 yr until the first supernovae (SNe) occur, and some 10^7 yr till the maximum of SN activity is reached. These time-scales are comparable to the duration of starbursts of about $10^7 - 10^8$ yr (Rieke et al. 1980; van den Broek et al. 1991; Bernlöhr 1993) and should therefore result in a time delay between the maximum emission of the FIR and the radio emission. Furthermore, during a starburst the intensity of the radiation field changes with time in a significant way. Little is known about variations of the magnetic field energy density. The ratio of these two parameters that determine the major radiative losses of the cosmic ray (CR) electrons (inverse Compton and synchrotron losses) is crucial for the total synchrotron emission of a galaxy.

The aim of this paper is to understand why, in spite of the above considerations, the FIR/radio ratio is observed to be very constant in starburst galaxies, and, more importantly, to use this observational fact to find constraints for starburst models. The paper consists of two parts: In the first part (Sects. 2 and 3), we present data for two large samples of galaxies, a starburst sample and a control sample, in order to investigate whether the FIR/radio ratio shows any dependence on the star-formation activity. In the second part (Sects. 4-6) we present a model for the FIR and the radio emission in a starburst in order to interprete the observational results. Section 7 summarizes our conclusions.

---

* Present address: Osservatorio Astrofisico di Arcetri, Largo E. Fermi 5, I-50125 Florence, Italy

Send offprint requests to: H.J. Völk

2. The sample

Both the sample of starburst galaxies and the control sample are selected from the list of UGC galaxies which are surveyed with the Arecibo 300m telescope at 2.4 GHz (Dressel & Condon 1978) and were covered by IRAS in FIR . These galaxies form a complete sample (down to $\mathrm{m_B} = 14.5$) of a local galaxy population, which have been studied by Franceschini et al. (1988a,b) for the radio and FIR luminosity functions.

It has been well established that non-Seyfert Markarian galaxies (Huchra 1977; Balzano 1983; Xu & De Zotti 1989; Mazzarella et al. 1991) and interacting galaxies (Larson & Tinsley 1978; Kennicutt et al. 1987; Telesco et al. 1988; Xu & Sulentic 1991) have on average significantly higher current star-formation rates than standard galaxies like the Milky Way. Therefore we select these galaxies for our starburst galaxy sample. It includes those galaxies classified in the UGC catalog (Nilson 1973) as peculiars, double, trible, or multiple systems, and galaxies identified by Markarian and collaborators as having ultraviolet excesses (see Mazzarella & Balzano 1986 for a review). Galaxies with active galactic nuclei (e.g. Seyfert galaxies) are not considered. The region of low galactic latitude ($|\mathrm{b}| < 30°$) is avoided in order to minimize the influence of Galactic extinction. Virgo galaxies listed in the VCC catalog (Binggeli et al. 1985) are excluded, because in clusters galaxies may have additional radio emission mechanisms other than the star-formation alone (Gavazzi et al. 1991; Völk & Xu 1994). There are 133 objects in the starburst galaxy sample.

The control sample includes spiral galaxies which are at high Galactic latitude ($|\mathrm{b}| > 40°$), and from the morphological types Sa through Sd in the UGC catalog. The sample excludes Virgo cluster, Markarian, as well as Seyfert galaxies. Galaxies catagorized simply as 'S' are not included, because the probability that they are misclassified early types is relatively high. There are 397 spirals in the control sample.

For the majority of objects in both samples, fluxes at 60μm and 100μm are taken from the Second Version IRAS Point Source Catalog. The exceptions are those extended (size $> 5'$) and faint ($f_{60\mu\mathrm{m}} < 0.6$ Jy) sources listed in the catalog of IRAS Faint Source Survey (FSS) fluxes of CfA galaxies (Thuan & Sauvage, 1992), for which the data are taken from Thuan & Sauvage (1992). For 133 objects in the starburst sample, 113 are detected at both 60μm and 100μm, corresponding to a detection rate of 85%. For the control sample, 329 are detected out of 397 objects, i.e. a detection rate of 83%. The integrated flux in the wavelength range 42.5 — 122.5 μm, S_{FIR} , or its upper limit, is calculated from the IRAS fluxes (limits) according to Helou et al. (1988). Radio fluxes at 2.4 GHz are taken from the Arecibo survey data (Dressel & Condon 1978). Fourty-six objects in the starburst sample and 92 in the control sample are detected in radio, corresponding to detection rates of 35% and 23%, respectively. For an overwhelming majority of sources in our samples, the total "face-on" blue magnitude $\mathrm{B_T^0}$, corrected for Galactic extinction, inclination effect and for redshift, can be found in the Third Reference Catalog (RC3) (de Vaucouleurs et al. 1991). For a few exceptionals whose $\mathrm{B_T^0}$ are not available, the blue magnitude is simply taken from the photographic magnitude given in UGC and corrected for the Galactic extinction calculated using the formula given in RC3. Taking $\mathrm{H_0} = 75\mathrm{kms^{-1}Mpc^{-1}}$, the distances are calculated from the recession velocities after correcting for the Virgocentric flow (Aaronson et al. 1982).

3. Statistical results

Fig. 1a. The FIR and the radio luminostities for the starburst sample. Upper limits are indicated by arrows.

In the statistical analysis carried out in this section, we use the so called 'survival technique' (Schmitt 1985; Feigelson & Nelson 1985) to exploit the information carried by the upper limits.

We plot in Figs. 1a and 1b the logarithms of the radio intensities versus the logarithms of the FIR luminosities for the starburst sample and for the control sample, respectively. The crosses are detected data, and the arrows denote the upper limits. Both samples show tight correlations between the FIR and the radio luminosities: the linear correlation coefficients are 0.90 and 0.88 for the starburst sample and the control sample, respectively. The slope of the log-log plot of the starburst sample is very close to unity: 0.98±0.01. On the other hand, the radio intensities increase slightly faster than the FIR luminosities for the normal spiral galaxies in the control sample:

Fig. 1b. The FIR and the radio luminostities for the control sample. Upper limits are indicated by arrows.

the slope is equal to 1.09±0.01 in Fig. 1b. In both plots, no galaxy is detected to seriously violate the correlation.

Similar to the q parameter defined by Helou et al. (1985), we introduce a parameter $q_{2.4\mathrm{GHz}}$:

$$\mathrm{q}_{2.4\mathrm{GHz}} = \log[(\mathrm{S}_{\mathrm{FIR}}/3.75\ 10^{12})/\mathrm{S}_{\nu}(2.4\mathrm{GHz})] \tag{1}$$

For the starburst sample, the mean of the $q_{2.4\mathrm{GHz}}$ is 2.40 ± 0.03, while for the control sample it is 2.52 ± 0.02. The statistical dispersion of the logarithm of the FIR/radio ratio, calculated using the survival technique, is $\sigma = 0.22$ for the starburst sample, and $\sigma = 0.21$ for the control sample. Therefore, although the $q_{2.4\mathrm{GHz}}$ value of the starburst sample is slightly lower than the control sample, the difference is within the dispersion.

An important question in this study is: does the FIR/radio ratio depend on the starburst strength? In principle, the starburst strength can be defined either via the FIR–to–blue luminosity ratio or via the radio–to–blue luminosity ratio. Both reflect, approximately, the ratio between the star-formation rates averaged over the last $\sim 10^8$ yr, s_8, and the last $\sim 3 \times 10^9$ yr, s_9, respectively (Xu et al. 1994). However, there is a trivial dependence (positive) of the FIR–to–radio ratio on the FIR–to–blue ratio, because the FIR luminosity is involved in both ratios. Similarly, a trivial dependence (negative) exists between the FIR–to–radio ratio and the radio–to–blue ratio. In order to minimize this artificial effect, we introduce a starburst strength indicator SB invoking both ratios:

$$\begin{aligned}\mathrm{SB} =\, & 0.5 \times \left[\left(\log\left(\frac{\mathrm{L}_{\mathrm{FIR}}}{\mathrm{L}_{\mathrm{B}}}\right) - \langle\log\left(\frac{\mathrm{L}_{\mathrm{FIR}}}{\mathrm{L}_{\mathrm{B}}}\right)\rangle\right) + \right. \\ & \left.\left(\log\left(\frac{\mathrm{P}_{2.4\mathrm{GHz}}}{\mathrm{L}_{\mathrm{B}}}\right) - \langle\log\left(\frac{\mathrm{P}_{2.4\mathrm{GHz}}}{\mathrm{L}_{\mathrm{B}}}\right)\rangle\right)\right]\end{aligned} \tag{2}$$

Fig. 2. The logarithmic ratio of the FIR–to–radio luminostity, $q_{2.4\mathrm{GHz}}$, and the indicator of the starburst strength, SB, defined in Eq. 2, for the starburst sample

Fig. 3. $q_{2.4\mathrm{GHz}}$ and the logarithm of the FIR colour, $\log f_{60\mu\mathrm{m}}/f_{100\mu\mathrm{m}}$, for the starburst sample

where $\langle\log\left(\frac{\mathrm{L}_{\mathrm{FIR}}}{\mathrm{L}_{\mathrm{B}}}\right)\rangle = -0.47 \pm 0.02$ and $\langle\log\left(\frac{\mathrm{P}_{2.4\mathrm{GHz}}}{\mathrm{L}_{\mathrm{B}}}\right)\rangle = -15.70 \pm 0.05$ are the means of the logarithms of the FIR–to–blue and of the radio–to–blue luminosity ratios of the *control* sample. A mean SB of 0.46±0.05 is found for the starburst sample, indicating that on average the s_8–to–s_9 ratio is a factor of 2.9±0.4 higher than that of the normal spirals in the control sample, consistent with previous studies (Kennicutt et al. 1987; Xu & Sulentic 1991).

Fig. 2 shows $q_{2.4GHz}$ vs SB for 113 objects in the starburst sample. The other twenty sources undetected either in the FIR or in the radio are dropped because no constraint can be imposed on their $q_{2.4\rm GHz}$ values. No correlation is found in this diagram. The two galaxies with the highest SB values show very normal $q_{2.4\rm GHz}$. The variation of the FIR–to–blue and the radio–to–blue ratios, so the SB, may be due to the variation of the extinction, in addition to the depence on the starburst strength. In order to verify the results obtained in Fig. 2, we plot in Fig. 3 the dependence of $q_{2.4\rm GHz}$ on another – extinction-free – starburst indicator, namely the $\log f_{60\mu m}/f_{100\mu m}$, for the same galaxies as in Fig. 2. As pointed out by Xu & De Zotti (1989) and by Bothun et al. (1989), $\log f_{60\mu m}/f_{100\mu m}$ is tightly associated to the high mass star-formation rate of galaxies, and the galaxies with the strongest starbursts usually show the highest $\log f_{60\mu m}/f_{100\mu m}$ values. Again, we do not detect any dependence of $q_{2.4\rm GHz}$ on this starburst indicator. Therefore, we conclude that the strength of the starburst does not introduce any siginificant influence on the FIR–to–radio ratio.

4. The starburst model

4.1. Star formation during a starburst

In the model we describe the starburst galaxy as the sum of two components: a starburst population with a star formation rate (SFR) $\Psi_{\rm SB}(t)$ changing on short time-scales and a background population whose SFR Ψ_{bg} is constant in time. The total SFR is the sum of both components, $\Psi(t)=\Psi_{\rm SB}(t)+\Psi_{\rm bg}$. The SFR of the starburst population is parametrized in the following way:

$$\Psi_{\rm SB}(t)=\begin{cases}\Psi_0\ \exp^{t/\tau_{\rm grow}} & \text{for } t<0\\ \Psi_0\ \exp^{-t/\tau_{\rm SB}} & \text{for } t\geq 0\end{cases} \tag{3}$$

where $\tau_{\rm grow}$ and $\tau_{\rm SB}$ are the time-scales of the increase and the decrease of the SFR. The ratio between the maximum SFR of the starburst population and the background population $a=\Psi_0/\Psi_{\rm bg}$ is a measure of the starburst strength. An upper limit for a can be estimated from the total amount of molecular gas available. The SFR of the background population can be estimated by assuming that the total amount of gas present is used up in about 10^{10} yr. Then we can estimate an upper limit of a by:

$$a=\Psi_0/\Psi_{\rm bg}\leq\frac{10^{10}\cdot x}{\tau_{\rm SB}} \tag{4}$$

where x is the fraction of molecular gas available for the starburst. In a nuclear starburst, about $20-30\%$ of the total amount of gas is in the nucleus and therefore available for the starburst (Bernlöhr 1992). The efficiency of the conversion of gas to stars can reach in starburst galaxies 50% (e.g. Rieke et al. 1980). With these numbers we derive $x=0.1-0.15$. Thus, e.g., for $\tau_{\rm SB}=10^7$ yr, an upper limit for a is about 100.

The Initial Mass Function (IMF), $\Phi(m)$, which determines the mass distribution of the stars produced, is described by a power-law

$$\Phi(m){\rm d}m=m^{-\gamma}{\rm d}m \tag{5}$$

with an upper mass limit $m_u=100\,{\rm M}_\odot$ and a lower mass limit $m_{\rm l}=1\,{\rm M}_\odot$ (stars less massive than that are neither of importance for the FIR nor the radio emission). We adopt $\gamma=2.7$, in agreement with Scalo (1986) and the more recent results of Basu and Rana (1992). In addition, we considered the effect of changes in the slope of the IMF and $m_{\rm l}$.

4.2. FIR emission

The FIR luminosity is calculated as

$$L_{\rm FIR}(t)=\int_{m_l}^{m_u}{\rm d}m\Phi(m)L(m)P(m)\zeta(m)\int_{t-\tau(m)}^{t}{\rm d}t\Psi(t) \tag{6}$$

where $\tau(m)$ is the stellar main-sequenze life-time, $L(m)$ the stellar luminosity (taken from Cox et al. 1988 and Cox et al. 1986), $P(m)$ the fraction of light absorbed by the dust and $\zeta(m)$ the fraction of the absorbed light that is reemitted in the IRAS 40–120 μm band. Here, we parametrize the last two parameters in the same way as explained in detail in Lisenfeld et al. (1995): For massive, ionizing stars ($m>20\,{\rm M}_\odot$) we assume $P(m)=0.6, \zeta(m)=0.5$. The radiation transfer of the non-ionizing emission of the intermediate massive stars ($5\,{\rm M}_\odot<m<20\,{\rm M}_\odot$) and the old stars ($1\,{\rm M}_\odot<m<5\,{\rm M}_\odot$) is approximated by an infinite parallel-slab geometry in which dust is homogenously mixed with the stars. We assume $A_V=1.5$ for the starburst population (Bernlöhr 1993) and $A_V=0.2$ for the background population (Lisenfeld et al. 1995; Xu & Buat 1995). We make the further simplification that the radiation of the intermediate massive stars is absorbed according to the dust opacity in the UV (2000 Å) and the radiation of the old stars according to the dust opacity in the blue (4400 Å).

Finally we split the FIR luminosity into the emission coming from H II regions, $L_{\rm FIR}^{\rm HII}$, and the diffuse emission $L_{\rm FIR}^{\rm diff}$, by assuming that stars more massive than 20 ${\rm M}_\odot$ are responsible for the dust heating in H II regions, and less massive stars for the diffuse dust heating.

4.3. Radio emission

The radio emission consists of thermal bremsstrahlung and of synchrotron emission. The thermal radio emission is proportional to the total number of Lyman continuum photons $N_{\rm Lyc}$ emitted by the stars:

$$P_{\rm therm}(\nu)=1.08{\cdot}10^{-33}\left(\frac{N_{\rm Lyc}}{\rm phot\,s^{-1}}\right)\left(\frac{\nu}{\rm GHz}\right)^{-0,1}[{\rm W/Hz}] \tag{7}$$

(e.g. Condon 1992) where we have assumed that the fraction of Lyman continuum photons directly absorbed by the dust is $f = 0.2$ and the electron temperature in the H II region $T_{\rm e} = 7000$ K. The total number of Lyman continuum photons is calculated as:

$$N_{\rm Lyc} = \int_{m_{\rm l}}^{m_{\rm u}} {\rm d}m\phi(m)\tilde{n}_{\rm lyc}(m) \int_{t-\tau(m)}^{t} {\rm d}t\Psi(t) \qquad (8)$$

where $\tilde{n}_{\rm Lyc}(m)$ is the production rate of Lyman continuum photons of a star of mass m, taken from Güsten & Mezger (1983).

In order to calculate the synchrotron emission in a starburst a time-dependent equation has to be solved. The details are described in the Appendix. Here we will only outline the most important features. Several processes are taken into account: We assume that the CR electrons are accelerated in shocks of SN remnants. Then they propagate into the galactic disk and halo losing their energy radiatively through inverse Compton and synchrotron losses. Since the radiation field in a starburst is very strong, the inverse Compton losses of the electrons are very high. This has the effect of shortening their radiative life-time, $\tau_{\rm loss}$, and therefore of decreasing the temporal shift between the FIR and the synchrotron radiation. (In a radiation field which is, for example, a factor of 10 higher than in the Galaxy, i.e. about 10 eV cm^{-3}, the life-time is $\tau_{\rm loss} \approx 10^6$ yr.) On the other hand, a high radiation field lowers the synchrotron emission itself, because the number density of electrons at a given energy is lowered (see Appendix). Therefore, during a starburst – if the magnetic field stays constant – the synchrotron emission is a sensitve function of the radiation field and therefore of the starburst strength. In particular it is very low during the phase of most active star-formation.

4.4. Starburst strength parameter SB

In order to compare our model with the data displayed in Fig. 3, we compute in the model the starburst parameter SB. The blue luminosity is obtained by assuming that the stellar emission is a blackbody spectrum. We obtain for the background, steady state population of the galaxy within our model: $\langle \log \left(\frac{L_{\rm FIR}}{L_{\rm B}}\right) \rangle = -0.34$ and $\langle \log \left(\frac{P_{2.4\rm GHz}}{L_{\rm B}}\right) \rangle = -15.48$. The model predictions are in rather good agreement with the mean values of the control sample. The small difference between model and data of $\langle \log \left(\frac{L_{\rm FIR}}{L_{\rm B}}\right) \rangle$, might be due to a slight overestimate of the average galactic extinction or due to the crude model assumptions (e.g. blackbody emission of stars). In the model $P_{2.4\rm GHz}$ for the background population is calculated from the model result for $L_{\rm FIR}$ and the mean value of $q_{2.4\rm GHz}$ of the control sample. Therefore the model prediction for $\langle \log \left(\frac{P_{2.4\rm GHz}}{L_{\rm B}}\right) \rangle$ is simply a combination of $\langle \log \left(\frac{L_{\rm FIR}}{L_{\rm B}}\right) \rangle$ (model), and $q_{2.4\rm GHz}$ (control sample).

The value of SB depends very sensitively on the extinction. The extinction in the starburst region is most likely higher than for the background population. We assumed $A_V = 1.5$, which is the typical internal extinction of the H II regions in nearby galaxies (Kennicutt 1983), and at the same time consistent with the average A_V found for the Markarian galaxies by Xu & De Zotti (1989).

In reality it seems plausible that some galaxies have an even higher extinction, explaining the large range in SB found for the starburst sample. The extinction mainly has an influence on SB, through L_B, and hardly on the FIR emission (see Fig. 9) because even for the value of A_V assumed for the background population ($A_V = 0.2$) the galaxies are optically thick for the nonionizing UV light which is the main heating source for the dust (Xu 1990).

5. Variation of $q_{2.4\rm GHz}$ during a starburst

In order to show the general features of the temporal evolution of $q_{2.4\rm GHz}$ during a starburst, we display in Fig. 4 the variation of $q_{2.4\rm GHz}$ during a starburst with a timescale $\tau_{\rm SB} = 10^7$ yr and $\tau_{\rm grow} = 0$ for different starburst strengths, and in the Figs. 5 and 6 separately the temporal evolution of the FIR and the radio emission.

Fig. 4. The ratio between the FIR and the radio emission at 2.4 GHz, $q_{2.4\rm GHz}(t)$, is shown as a function of time for $\tau_{\rm SB} = 10^7$ yr, $\tau_{\rm grow} = 0$, B =const, $a = \Psi_0/\Psi_{\rm bg} = 100$ (full line), $a = 50$ (dashed line), and $a = 25$ (dotted line). The dash-dotted line shows $q_{2.4\rm GHz}$ for a steady state galaxy.

The temporal variation of $q_{2.4\rm GHz}$ can be split into 3 phases: In the early phase (phase I; here: until ≈ 50 Myr) $q_{2.4\rm GHz}(t)$ is higher than the steady state value at this frequency. In this phase the emissions from H II regions dominate the total FIR and radio emission (see Figs. 5 and 6).

Fig. 5. For a starburst with $a = 100$ and otherwise the same parameters as in Fig. 4 the FIR emission (full line) is shown as a function of time. The FIR emission from H II regions (dashed line) and the FIR emission from diffuse dust (dotted line) are shown separately. The dash-dotted line describes the FIR emission from the background galaxy.

Fig. 6. For $a = 100$ and otherwise the same parameters as in Fig. 4 the radio emission during the starburst is shown (full line), devided into thermal bremsstrahlung (dashed line) and synchrotron emission (dotted line). The dash-dotted line describes the radio emission from the background galaxy.

With respect to the FIR emission, this is due to the high relative abundance of massive stars. For the synchrotron emission other reasons are more important: First of all, it takes serveral 10^6 yr until the first SN explosions occur. More important, however, is the fact that during the first serveral 10^7 yr the synchrotron emission is strongly suppressed (see Fig. 6) due to the strong inverse Compton losses caused by a high radiation field. It is worth to note that only because of the presence of the thermal radio emission and because the two ratios ($\log(L_{\rm FIR}^{\rm HII}/P_{\rm therm})$ and $\log(L_{\rm FIR}^{\rm diff}/P_{\rm syn})$ are relatively similiar no major difference of $q_{\rm 2.4GHz}$ with respect to a steady state galaxy occurs in this phase.

In the next phase (phase II; here: between about $50 - 100$ Myr), $q_{\rm 2.4GHz}$ can be even lower than in a steady state. This is due to the time delay between the SN explosions and the FIR emission: it leads to a maximum of the radio emission at a time when the FIR emission is already in its declining phase.

In the last phase (phase III; here: after about 100 Myr) the opposite temporal effect occurs: The synchrotron radiation has already decreased to the steady state value – or even below because the inverse Compton losses are still higher than before the starburst – but the FIR emission is still high due to dust heating by low-mass ($m = 1 - 3\,{\rm M}_\odot$) stars. Therefore during this phase $q_{\rm 2.4GHz}$ is higher than the steady state value and depends sensitively on $a = \Psi_0/\Psi_{\rm bg}$. In this phase the galaxy is already completely in the post-starburst phase.

Fig. 7. The model result for the same parameters as in Fig. 4 (with $a = 100$) are compared to the data. The full line shows the model results for SB and $q_{\rm 2.4GHz}$ for the time interval between $t = 0$ and $t = 10^9$ yr with the arrow indicating the direction of increasing time.

The deviations of $q_{\rm 2.4GHz}$ from the steady state value in the various phases are therefore either due to the different time-scales of the FIR and the radio emission or due to the high inverse Compton losses experienced by the electrons.

In Fig. 7 the model results are compared to the data. It can be seen that in phase I the model predictions for $q_{2.4\mathrm{GHz}}$ lie substantially above the data. In the following we will try to find parameters that reduce the temporal variation of $q_{2.4\mathrm{GHz}}$ to a minimum and fit the data.

6. Constraints on starburst parameters by comparison with the observations

6.1. Young starburst (phase I): Fast increase of the magnetic field?

The main reason for the high model value of $q_{2.4\mathrm{GHz}}$ during the early phase is a lack of synchrotron radiation due to high inverse Compton losses. The radio emission during the first $\sim 2 \times 10^7$ yr is therefore – if the magnetic field remains constant – practically completely thermal (Fig. 6). This has not been observed, however: Van den Driel et al. (1991) determined the thermal radio fraction of a sample of starburst galaxies and derived only 40% at 5 GHz (corresponding to about 30% at 2.4 GHz). A possibly very high thermal fraction should furthermore be noticeable in a flat radio spectrum ($P_{\mathrm{rad}}(\nu) \propto \nu^{-0.1}$) which has not been observed either.

The suppression of the synchrotron emission will be substantially diminished if the magnetic field increases rapidly, already in phase I. The behaviour of the magnetic field in a starburst has not been well studied yet, but it seems plausible that the field increases. Ko & Parker (1989) proposed a model in which the increase of interstellar turbulence due to a high SFR activates a turbulent galactic dynamo. An alternative process to increase the magnetic field in a starburst could be the compression by SN shocks of the ionized gas in which the field is frozen. A third field enhancement process could be the systematic dynamo effect due to a commencing galactic wind as we may be observing in M 82 or even at the centre of our Galaxy.

In each of the three scenarios the increase of the magnetic field is ultimately caused by the star formation. After the end of the starburst, the magnetic field enhancement stops and the field dissipates slowly. Therefore we will tentatively parametrize the temporal variation of the magnetic field as:

$$B(t)^2 \begin{cases} \propto L_{\mathrm{FIR}}(t) & \text{if } \frac{\partial L_{\mathrm{FIR}}}{\partial t} > 0 \\ = \text{constant} & \text{otherwise} \end{cases} \tag{9}$$

In Figs. 8 and 9 the results are shown. It can be seen that the magnetic field increase lowers substantially the value of $q_{2.4\mathrm{GHz}}$ in phase I and allows to fit the data.

We would like to stress that the results presented do not crucially depend on the exact parametrization of the magnetic field increase during phase I. The important point is a fast increase of the magnetic field. The time-scale of this increase has to be rather short ($\approx 10^7$) because a large magnetic field strength is required already in an early stage of the starburst. The time-scale for the dynamo activity has been estimated to be between 10^8

Fig. 8. $q_{2.4\mathrm{GHz}}$ is shown for $\tau_{\mathrm{SB}} = \tau_{\mathrm{grow}} = 10^7$ yr, $a = 100$ (dashed line), $\tau_{\mathrm{SB}} = \tau_{\mathrm{grow}} = 3 \times 10^7$ yr, $a = 50$ (full line) (both with $m_{\mathrm{l}} = 1\,\mathrm{M}_{\odot}$) and for $\tau_{\mathrm{SB}} = \tau_{\mathrm{grow}} = 3 \times 10^7$ yr, $a = 50$, $m_{\mathrm{l}} = 3\,\mathrm{M}_{\odot}$(dotted line). An increase of the magnetic field according to Eq. (9) has been taken into account in all three cases.

Fig. 9. In the same way as in Fig. 7 the model results and the data are compared. The parameters for the model are: $\tau_{\mathrm{grow}} = \tau_{\mathrm{SB}} = 3 \times 10^7$ yr, $a = 50$, $m_{\mathrm{l}} = 1\,\mathrm{M}_{\odot}$, $A_V = 1.5$ (full line). In the dashed line the result for $A_V = 5$ is shown in order to illustrate the influence of the extinction on the parameter SB.

(Ko & Parker 1989) and $> 10^9$ yr (Field 1993). Therefore a dynamo may be a too slow process for a starburst. However the alternative processes, such as outward "combing" of the field by a mass outflow or of field compression by SN shocks, would occur on the time-scale of stellar wind bubble evolution and SN activity. At least the wind activity is directly coupled to the FIR enhancement with delays of the order of a million years only. An example for this might be the nearby starburst galaxy M 82. It lies on the FIR/radio correlation (e.g. Wunderlich et al. 1987). Bernlöhr (1992) estimated that the starburst in M 82 has been active for $1 - 5 \times 10^7$ yr, i.e. M 82 is in our phase I. The fast galactic outflow from the starburst nucleus and the corresponding convective electron transport is consistent with the observed synchrotron emission and the SN rate (Völk et al. 1989).

Parker (1992) has argued that galactic dynamos can be driven by the pressure of cosmic rays and the subsequent reconnection of azimuthal field lines to produce poloidal fields. This process is competitive to our assumed extension of magnetic field lines to "infinity" by a wind. The point here is that also the above version of a galactic dynamo can more or less adiabatically follow the time variations in the production of cosmic rays, presumably in SNRs, as our data indeed suggest.

6.2. Evolved starburst (phase II): Time-scale

If the time-scale of the variation of the star formation rate is very short, i.e. roughly shorter than the time-scale for SN-explosions ($\sim 10^7$ yr, i.e. the life-time of SN progenitors), the maximum of the attendant synchrotron emission occurs at a time when the FIR emission, which has about the same time-scale as the starburst, has already decreased significantly. This results in a very low model value of $q_{2.4\mathrm{GHz}}$ (less than 3 σ below the steady state value). Therefore, in order to fit the data satisfactorily during this phase, $\tau_{\mathrm{grow}} + \tau_{\mathrm{SB}}$ has to be at least comparable to the SN time-scale, i.e. about 10^7 yr. Such time-scales are short enough to allow for repetitive bursts of star formation on time-scales of 10^8 yr as discussed by Krügel & Tutukow (1993). Our model results provided good fits to the data for time-scales longer than about 3×10^7 yr. These numbers are in agreement with other authors who found starburst time-scales between 2×10^7 and some 10^8 yr (Rieke et al. 1980; van den Broek et al. 1991; Bernlöhr 1993). We furthermore inferred a minimum time-scale for the increase of the SFR of $\tau_{\mathrm{grow}} \gtrsim 3 \times 10^7$ yr. This slow increase was necessary in order to provide a large enough magnetic field strength and SN rate in the early starburst phase.

6.3. Post-starburst (phase III): A higher low-mass cut-off of the IMF?

We also tested the effect of changes in the IMF, both of the slope k and the low-mass cut-off m_{l}. These two parameters are suggested by many authors to be different in a starburst in the sense that the star formation is likely to be biased towards massive stars (e.g. Rieke et al. 1980; Rieke et al. 1993; Bernlöhr 1992; Wright et al. 1988). For our model, the most noticeable influence of the IMF occurs in the post-starburst phase (III). When the canonical IMF (Eq. (5)) is assumed for the starburst, the enhancement in the FIR emission lasts significantly longer than the radio emission because of the dust-heating due to the A stars ($\sim 2\,\mathrm{M}_\odot$) produced in the burst. This is shown by a relatively high model value of $q_{2.4\mathrm{GHz}}$ in this phase (Figs. 4 and 8). A better agreement with the data can be obtained if a higher low-mass cut-off, i.e. $m_{\mathrm{l}} \sim 3\,\mathrm{M}_\odot$ (see Fig. 8), is adopted. A flatter slope will have a similar effect. Hence, our result seems also in favour of a top-heavy IMF for starbursts.

7. Summary and Conclusions

We have analysed and compared the FIR and radio data of a sample of interacting/Markarian galaxies (starburst sample) and a sample of normal galaxies (control sample) in order to test for the influence of the star formation activity on the FIR-to-radio ratio. A model for the FIR and the radio emission in a starburst was used to interprete the observational results and to derive constraints on starburst parameters. The following main conclusions could be drawn:

- The mean FIR-to-radio ratio, $q_{2.4\mathrm{GHz}}$, showed no significant difference between the starburst sample and the control sample and is independent of the starburst strength.
- The magnetic field is required to increase strongly on short time-scales ($\approx 10^7$ yrs) in order to maintain a sufficiently constant $q_{2.4\mathrm{GHz}}$ in the first $\approx 2 \times 10^7$ yr of a starburst. Otherwise the inverse Compton losses during this phase would lead to a very low synchrotron emission, resulting in a value of $q_{2.4\mathrm{GHz}}$ significantly higher than the observed one.
- The time-scale of the variation of the star-formation rate has to be longer than some 10^7 yr. Otherwise the different time-scales of the FIR and the radio emission produce large fluctuations in $q_{2.4\mathrm{GHz}}$.
- Our results favour a top-heavy IMF for starbursts (i.e. either a higher lower mass cut-off of $m_{\mathrm{l}} \sim 3\,\mathrm{M}_\odot$ or a flatter slope of the IMF) because this reduces the contribution of A stars to the dust heating, thus shortens the time-scale of the FIR emission and therefore improves the agreement with the data for the post-starburst (phase III).

Acknowledgements. We would like to thank M. Ko for helpful discussions. UL gratefully acknowledges the receipt of a stipend of the Max-Planck-Gesellschaft and of the Deutsche Forschungsgemeinschaft (DFG). HJV and CX acknowledge that part of their work in this paper has been done in the framework of the Sonderforschungsbereich 328 (Entwicklung von Galaxien) of the DFG.

Appendix : Synchrotron emission during a starburst

Assuming that the time-scale of the radiative energy losses is much shorter than the time-scale of diffusion, which is certainly a valid assumption for a starburst where the inverse Compton losses of the electrons are very large, we can neglect diffusion and describe the temporal evolution of the electron particle density $f(t,E)$ by the following equation:

$$\frac{\partial f(t,E)}{\partial t} = \left(\frac{E}{mc^2}\right)^{-x} q_{\rm SN}\nu_{\rm SN}(t) + \frac{\partial}{\partial E}\left\{b(t)\,E^2\,f(t,E)\right\} \qquad (A1)$$

where $(E/mc^2)^{-x}q_{\rm SN}\nu_{\rm SN}(t)$ is the source spectrum of the relativistic electrons with $\nu_{\rm SN}(t)$ as the supernova rate and $q_{\rm SN}$ as the number of relativistic electrons produced per supernova and per energy interval. The power law index of the source spectrum is taken as $x = 2.2$ (Völk et al. 1988). The energy losses $b(t) \propto c_1(U_{\rm rad}(t) + U_B(t))$ describe the inverse Compton and synchrotron losses which are proportional to the energy density of the radiation field $U_{\rm rad}$ and the energy density of the magnetic field $U_{\rm B}$, respectively.

The solution of Eq. (A1) for the starburst population is given by:

$$f_{\rm SB}(E,t) = \left(\frac{E}{mc^2}\right)^{-x} \cdot q_{\rm SN} \int_{\rm max(t_{start},t-\tau_{loss}(E,t))}^{t} {\rm d}t'\,\nu_{\rm SN}^{\rm SB}(t')\left(1 - E\int_{t'}^{t} b(t''){\rm d}t''\right)^{x-2}. \qquad (A2)$$

Here, $\tau_{\rm loss}(E,t)$ is the time-scale of the radiation losses of the electrons during the starburst which is defined by the relation:

$$E\int_{t-\tau_{\rm loss}(E,t)}^{t} b(t')dt' = 1. \qquad (A3)$$

The boundary condition is that at the beginning of the starburst, at $t = t_{\rm start}$ (which we approximate here as $t_{\rm start} = -4\times\tau_{\rm grow}$), the electron density $f_{\rm SB}(E, t_{\rm start}) = 0$. For the background population a similiar solution is derived. The solution for the electron density can be understood in the following way: SNe taking place between $t-\tau_{\rm loss}(E,t)$ and t contribute to $f(E,t)$. The contribution of SNe at a time t' gets a weight corresponding to the radiation losses that are relevant between t' and t. The higher the radiation losses, the lower is the number density of electrons in a particular energy range.

In order to calculate $f(E,t)$ from Eq. (A2), one has to know $\nu_{\rm SN}(t)$ and $b(t)$, the latter being proportional to $U_{\rm rad}(t) + U_B(t)$. The supernova rate $\nu_{\rm SN}(t)$ is calculated directly from the SFR given in Eqs. (3) and (5). The temporal evolution of the energy density of the radiation field, $U_{\rm rad}(t)$, is proportional to the bolometric luminosity $L_{\rm bol}(t)$ of the galaxy if the volume emitting the radition does not change significantly during the starburst:

$$U_{\rm rad}(t) = L_{\rm bol}(t)\cdot\frac{U_{\rm rad}^{\rm bg}}{L_{\rm bol}^{\rm bg}} \qquad (A4)$$

We take the radiation energy density of the steady state galaxy before the starburst $U_{\rm rad}^{\rm bg} = 1{\rm eV/cm}^3$, according to the value in our Galaxy. $L_{\rm bol}^{\rm bg}$, its bolometric luminosity, is derived from the model, assuming a constant SFR.

The temporal evolution of the magnetic field is parametrized according to Eq. (9). The energy density of the magnetic field in a steady state is taken as the Galactic value: $U_B^{\rm bg} = 1{\rm eV/cm}^3$ which corresponds to a magnetic field of $B^{\rm bg} = 6.3\mu$G.

Knowing the electron particle density $f(E,t)$, we can calculate the synchrotron radiation by:

$$P_{\rm syn}(\nu,t){\rm d}\nu = f(E(\nu),t)\left.\frac{{\rm d}E}{{\rm d}t}\right|_{\rm syn}\frac{{\rm d}E}{{\rm d}\nu}{\rm d}\nu \qquad (A5)$$

with $({\rm d}E/{\rm d}t)|_{\rm syn}$ as the energy loss by synchrotron radiation and ${\rm d}E/{\rm d}\nu$ given through:

$$\nu = \left(\frac{E}{mc^2}\right)^2\frac{\nu_{\rm G}(B)}{0.45} \qquad (A6)$$

(Longair 1994) with $\nu_{\rm G}$ being the gyrofrequency. This corresponds to the simplification that an electron of energy E emits the whole synchrotron radiation at the maximum frequency of the synchrotron spectrum.

In order to find the absolute normalization of the synchrotron radiation we scale the synchrotron radiation such that the FIR/radio ratio $q_{2.4{\rm GHz}}$ for the background population is equal to the observed average value of the control sample.

References

Aaronson M., Huchra J., Mould J., Schechter P., Tully R.B., 1982, ApJ 258, 64
Balzano V.A., 1983, ApJ 268, 602
Basu S., Rana R.C., 1992, ApJ 393, 373
Bernlöhr K., 1992, A&A 263, 54
Bernlöhr K., 1993, A&A 268, 25
Binggeli, B. Sandage A., Tammann G. A., 1985, AJ 90, 1681
Bothun G.D., Lonsdale C.J., Rice, W., 1989, ApJ 341, 129
Condon J.J., 1992, A&AR 30, 575
Condon J.J., Huang Z.P. Yin Q.F. 1991, ApJ 378, 65

Cox M.J., Eales S.A.E., Alexander P., Fitt A.J., 1988, MNRAS 237, 381

Cox P., Krügel E., Mezger P.G., 1986, A&A 155, 155

de Vaucouleurs G., de Vaucouleurs A., Corwin H. et al., 1991, Third Reference Catalog of Galaxies. New York, Springer-Verlag (RC3)

Dressel L.L., Condon J.J. 1978, ApJS 36, 53

Feigelson E.D., Nelson P.I. 1985, ApJ 293, 192

Field G., 1993, in: J. Franco, F. Ferrini, G. Tenorio-Tagle (eds.), Star Formation, Galaxies and the Interstellar Medium. Cambridge University Press, Cambridge

Franceschini A., Danese L., De Zotti G., Toffolatti L., 1988a, MNRAS 233,157

Franceschini A., Danese L., De Zotti G., Xu C., 1988b, MNRAS 233,157

Gavazzi G., Boselli A., Kennicutt R., 1991, AJ 101, 1207

Güsten R., Mezger P.G., 1983, Vistas in Astronomy 26, 159

Helou G., Soifer B.T., Rowan-Robinson M., 1985, ApJ 298, L7

Helou G. Khan I.R., Malek L., Boehmer L., 1988, ApJS 68, 151

Huchra J.P., 1977, ApJ 217, 928

Kennicutt R.C., 1983, ApJ 272, 54

Kennicutt R., Keel W., van der Hulst J., Hummel E., Roettiger K., 1987, AJ 93, 1011

Ko C.M., Parker E.N., 1989, ApJ 341, 828

Krügel E., Tutukov A.V., 1993, A&A 275, 416

Larson R.B., Tinsley B.M., 1978, ApJ 219, 46

Lisenfeld U., Völk H.J., Xu C., 1996, A&A 306, 677

Longair M.S., 1994, High Energy Astrophysics. Vol 2., Cambridge University Press

Mazzarella J.M., Balzano V.A., 1986, ApJS 62, 751

Mazzarella J.M., Bothen G.D., Borrosen T.D., 1991, AJ 101, 2034

Nilson P., 1973, Uppsala General Catalogue of Galaxies. Uppsala Astronomical Observatory, Uppsala (UGC)

Parker E.N., 1992, ApJ 401, 137

Rieke G.H., Lebofsky M.J., Thompson R.I., Low F.J., Tokunaga T., 1980, ApJ 238, 24

Rieke G.H., Loken K., Rieke M.J., Tamblyn P., 1993, ApJ 412, 99

Scalo J.M., 1986, Fundam. of Cosmic Research, 11

Schmitt J.H.M.M., 1985, ApJ 293, 178

Telesco C., Wolstencroft R., Done C., 1988, ApJ 329, 174

Thuan T.X., Sauvage M., 1992, A&AS 92, 749

van den Broek A.C., de Jong T., Brink K. 1991 A&A 246, 313

van den Driel W., van den Broek A.C., de Jong T., 1991 A&AS 90, 55

Völk H.J., Xu C. 1994, Infrared Phys. Technol. 35, 527

Völk H.J., Zank L.A., Zank G.P, 1988, A&A 198, 274

Völk H.J., Klein U., Wielebinski R., 1989, A&A 213, L12

Wright G.S., Joseph R.D., Robertson N.A., James P.A., Meikle W.P.S., 1988, MNRAS 233,1

Wunderlich E., Klein U., Wielebinski R., 1987, A&AS 69, 487

Xu, C., 1990, ApJ 365, L47

Xu C., Buat V., 1995, A&A 293, L65

Xu C., De Zotti G. 1989, A&A 225, 12

Xu C., Sulentic J.W. 1991, ApJ 374, 407

Xu C., Lisenfeld U., Völk H.J., Wunderlich E., 1994, A&A 282, 19

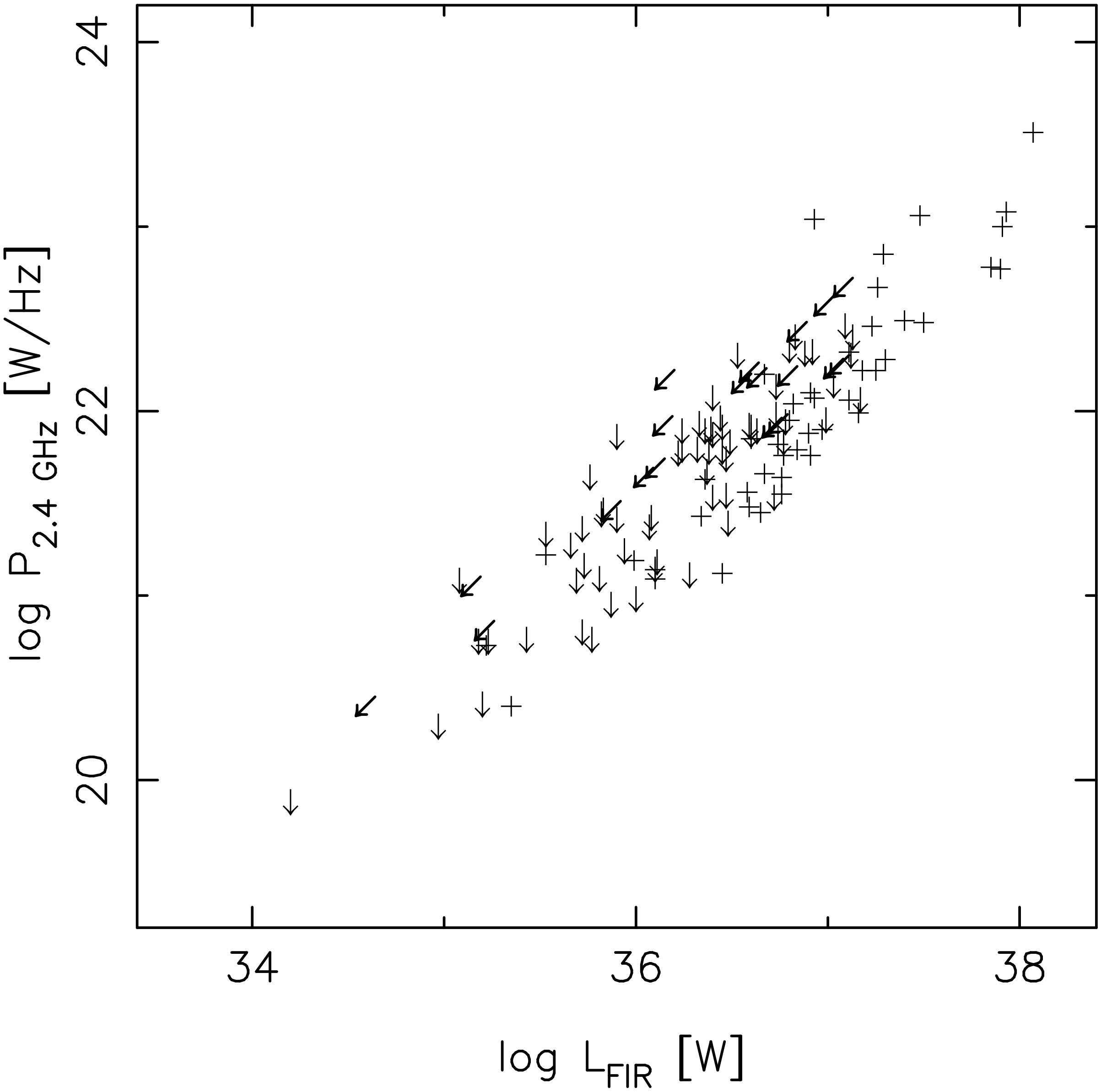
log P$_{2.4\ GHz}$ [W/Hz]
24
22
20
log L$_{FIR}$ [W]
34
36
38

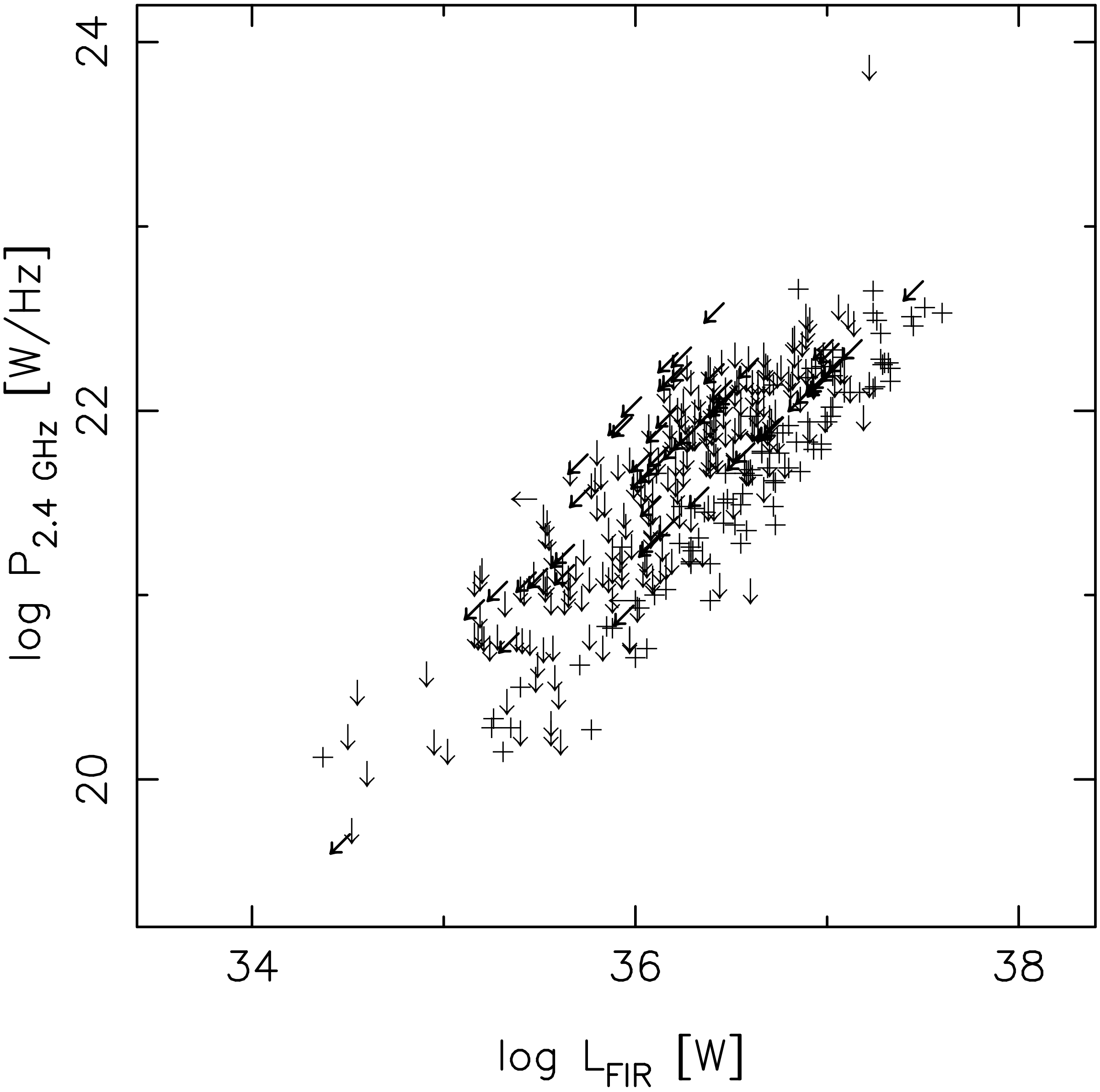

log P$_{2.4\ \mathrm{GHz}}$ [W/Hz]
24
22
20
34
36
38
log L$_{\mathrm{FIR}}$ [W]

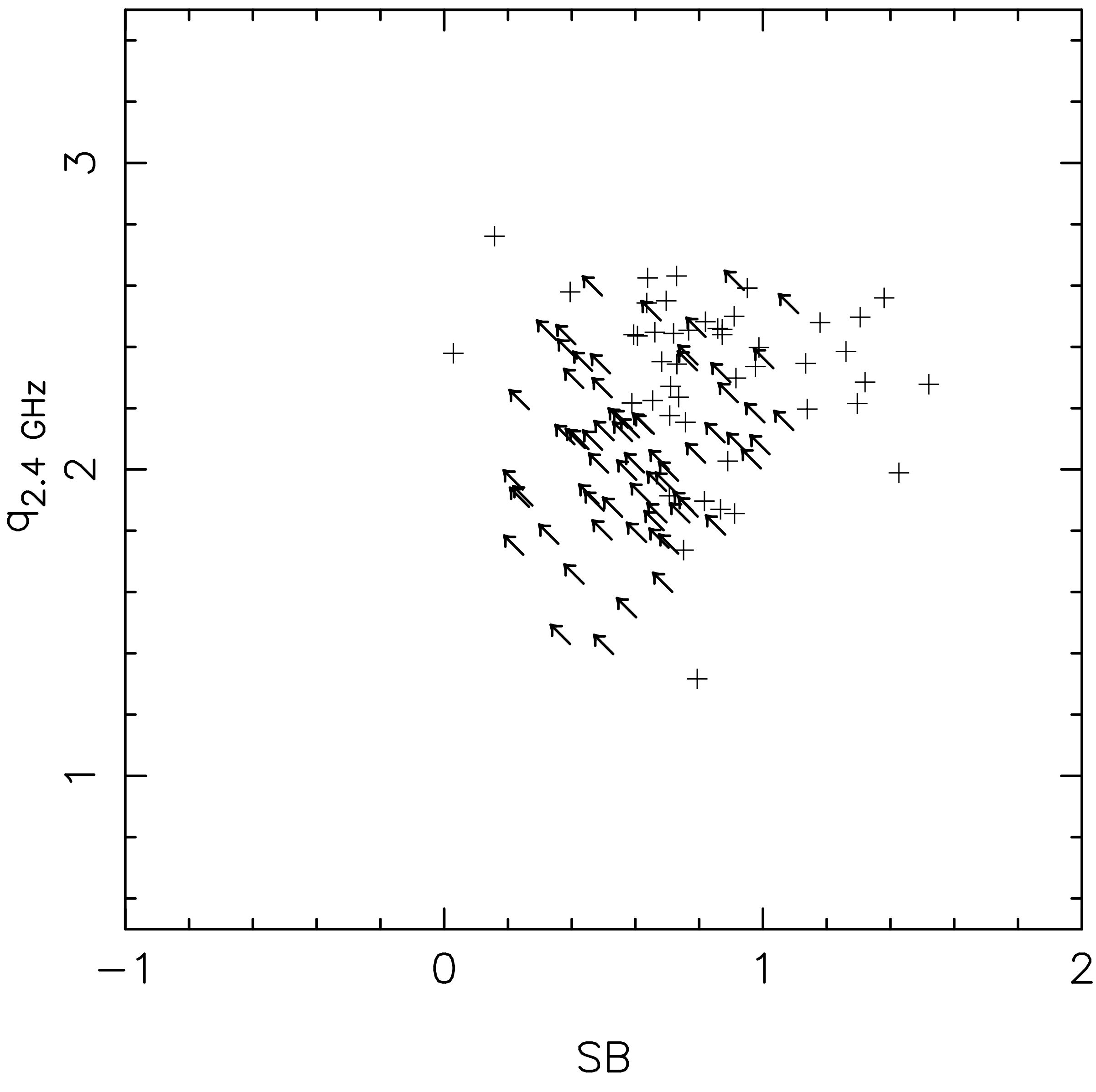

$q_{2.4\ \mathrm{GHz}}$
1
2
3
−1
0
1
2
SB

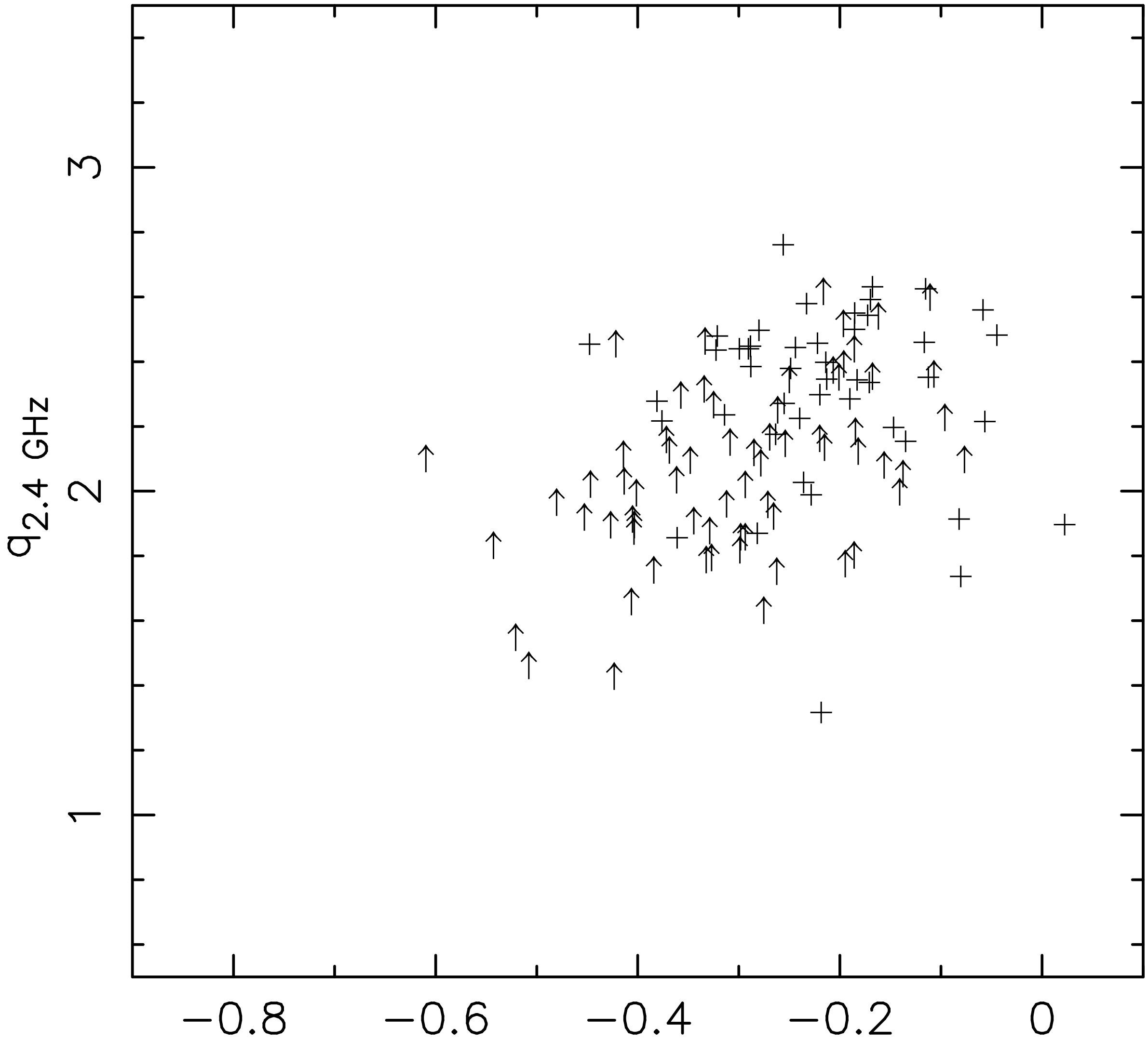

$q_{2.4\ \mathrm{GHz}}$
1
2
3
−0.8
−0.6
−0.4
−0.2
0
log $f_{60\mu m}/f_{100\mu m}$

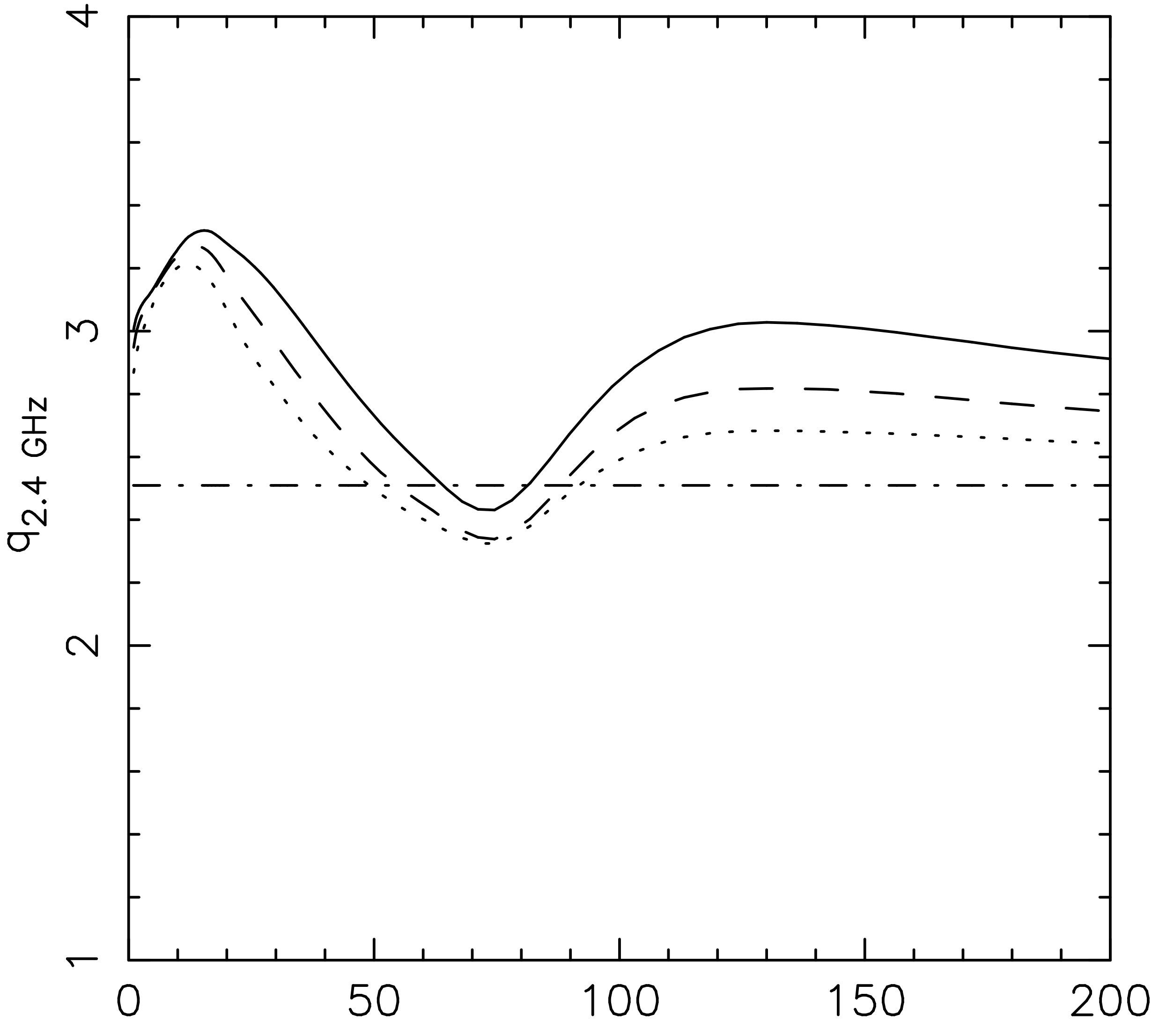
4
3
2
1
$q_{2.4\ \mathrm{GHz}}$
0
50
100
150
200
t [10^6 years]

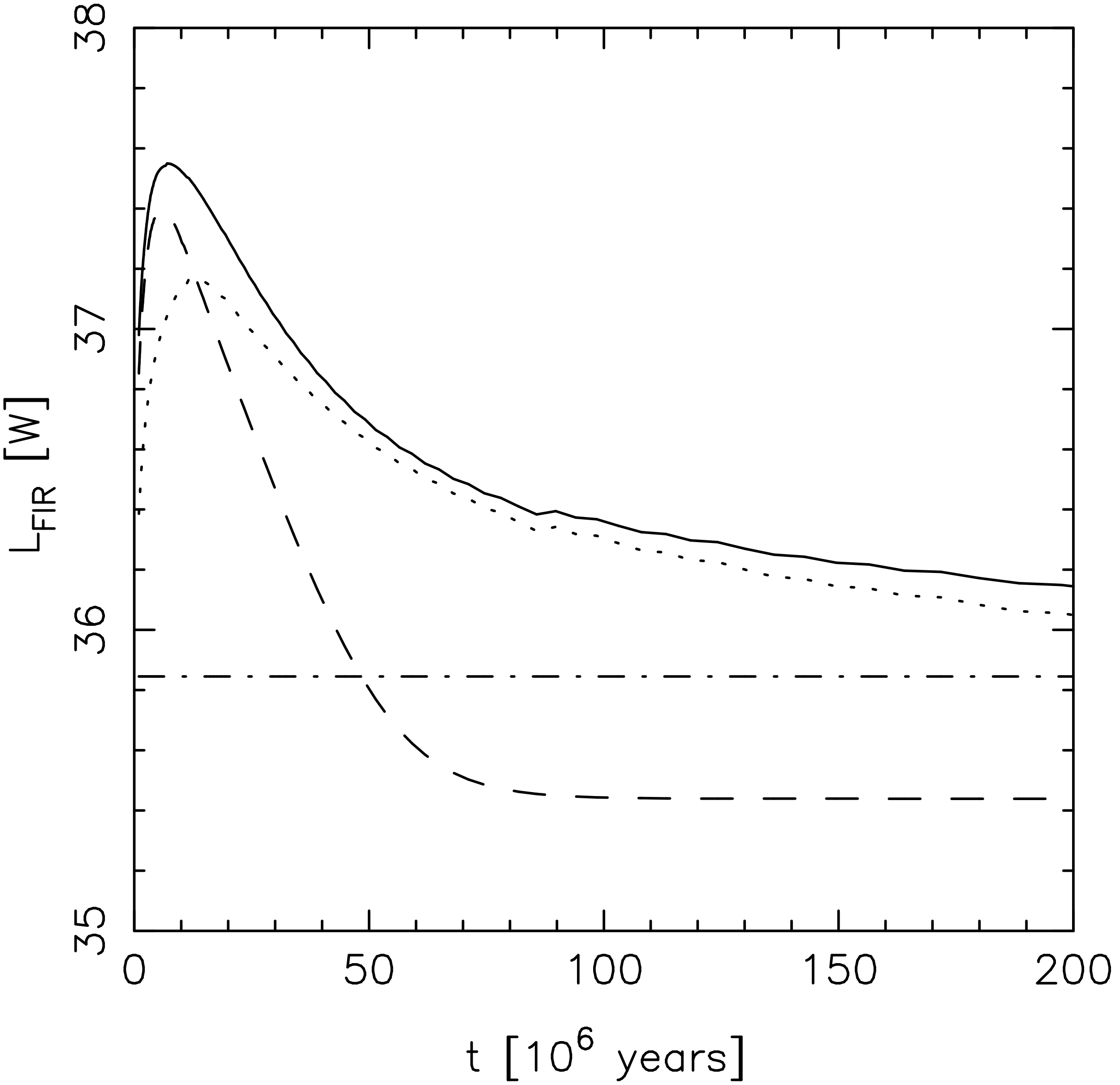

38
37
36
35
L_{FIR} [W]
0
50
100
150
200
t [10^6 years]

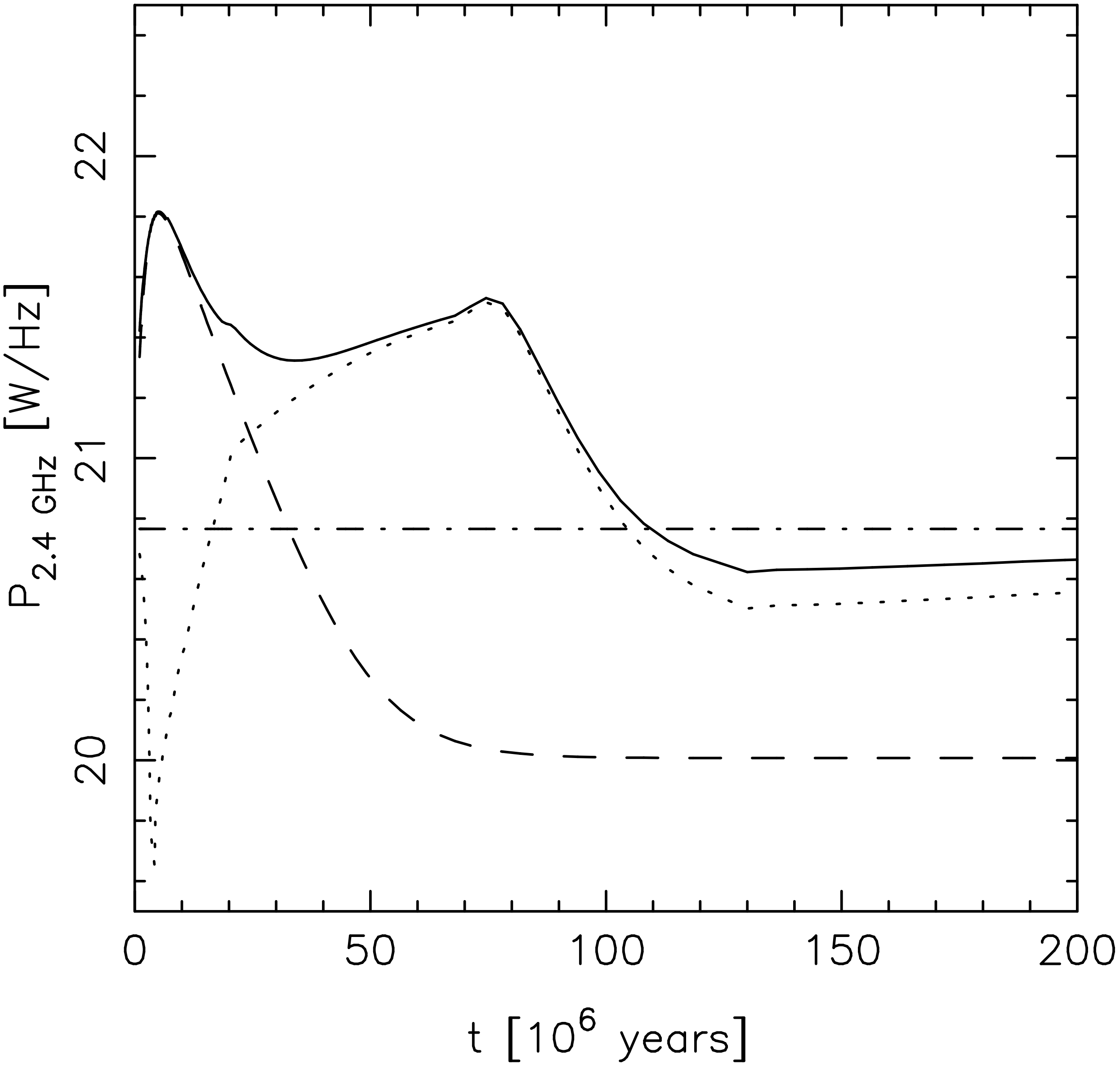
$P_{2.4\ \mathrm{GHz}}$ [W/Hz]
22
21
20
0
50
100
150
200
t [10^6 years]

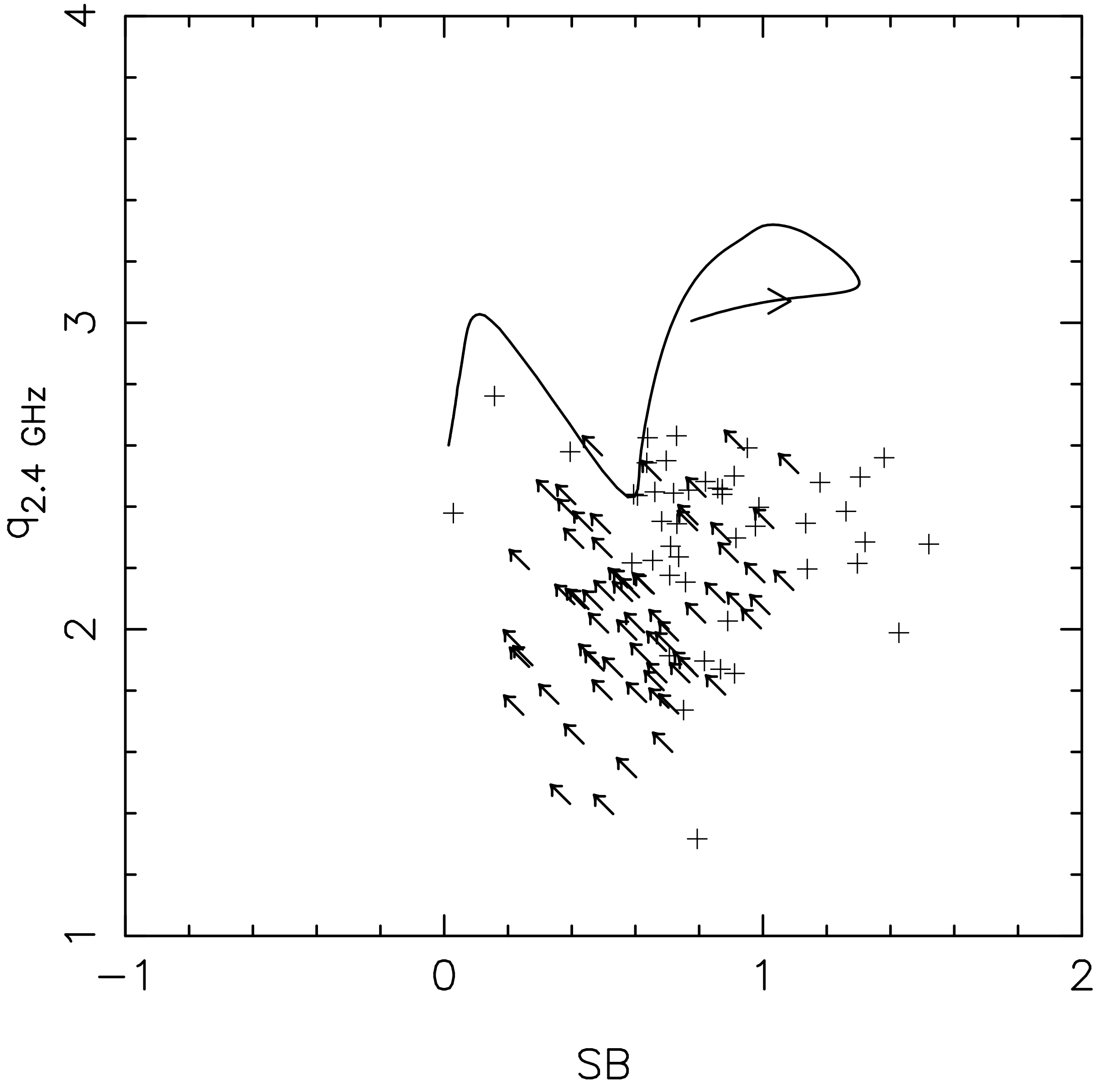

4
3
2
1
−1
0
1
2
q_{2.4 GHz}
SB

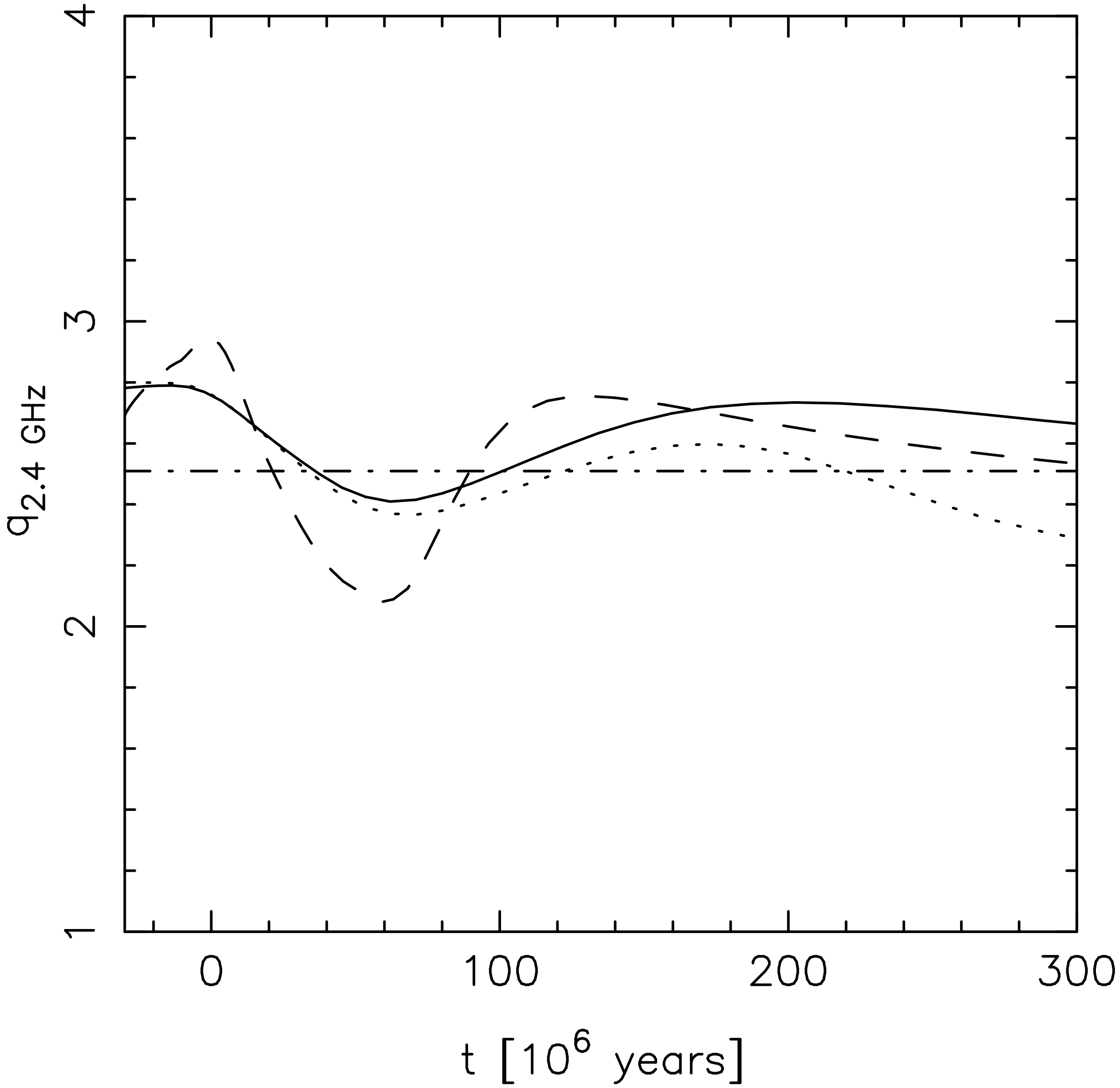
4
3
2
1
$q_{2.4\ \mathrm{GHz}}$
0
100
200
300
t [10^6 years]

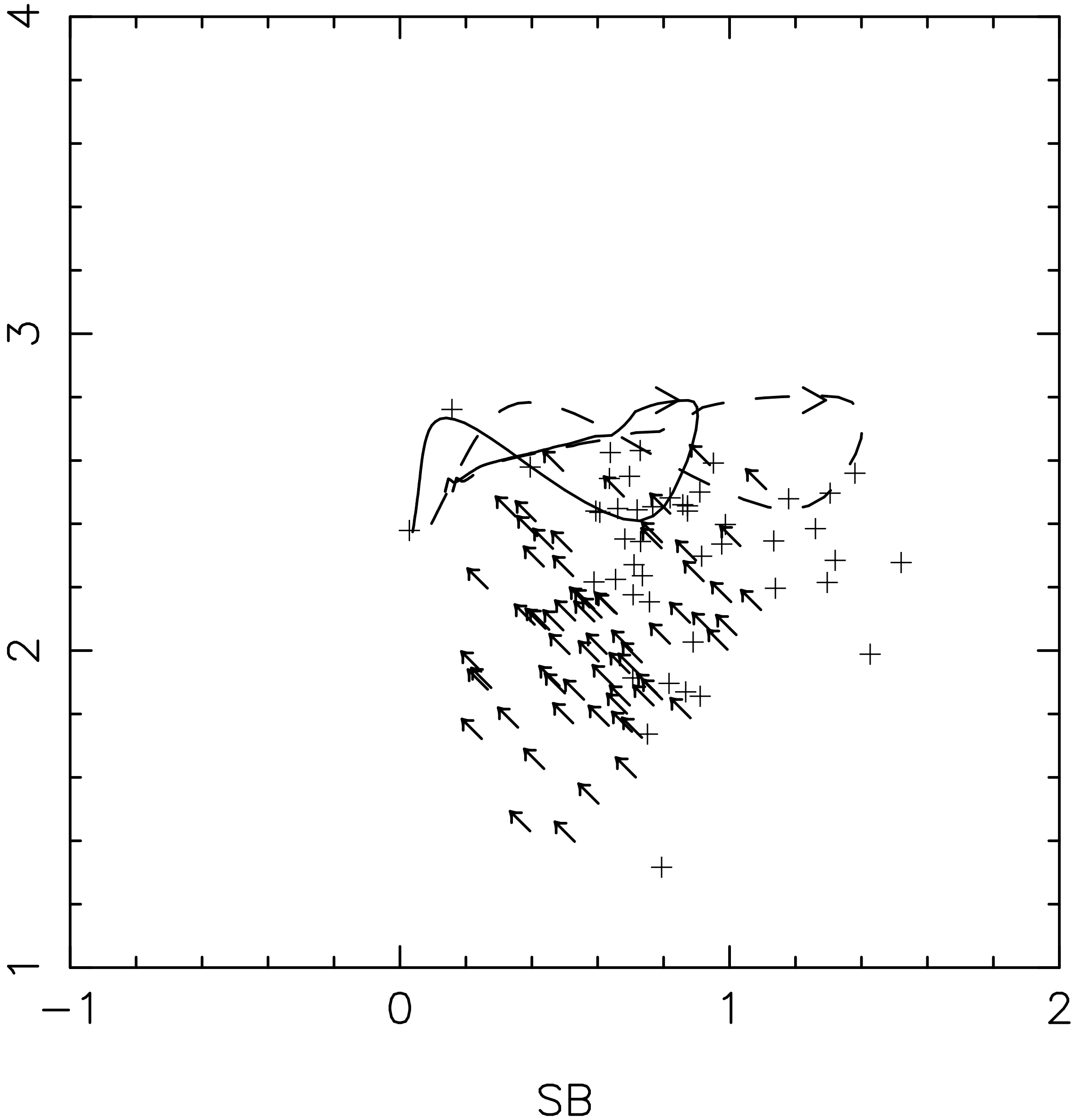

4
3
2
1
$q_{2.4\ \mathrm{GHz}}$
−1
0
1
2
SB